Chemical Transformations Drive Complex Self-Assembly of Uracil on Close-Packed Coinage Metal Surfaces (ACS Nano, volume 6, issue 3, pages 2477–2486, year 2012)

Anthoula C. Papageorgiou,[1, a)] Sybille Fischer,[1] Joachim Reichert,[1, b)] Katharina Diller,[1] Florian Blobner,[1] Florian Klappenberger,[1] Francesco Allegretti,[1] Ari P. Seitsonen,[2] and Johannes V. Barth[1]

[1)] *Physik Department E20, Technische Universität München, 85748 Garching, Germany*

[2)] *Physikalisch-Chemisches Institut der Universität Zürich, Winterthurerstrae 190, CH-8057 Zürich, Switzerland*

We address the interplay of adsorption, chemical nature, and self-assembly of uracil on the Ag(111) and Cu(111) surfaces as a function of molecular coverage (0.3 to 1 monolayer) and temperature. We find that both metal surfaces act as templates and the Cu(111) surface acts additionally as a catalyst for the resulting self-assembled structures. With a combination of STM, synchrotron XPS, and NEXAFS studies, we unravel a distinct polymorphism on Cu(111), in stark contrast to what is observed for the case of uracil on the more inert Ag(111) surface. On Ag(111) uracil adsorbs flat and intact and forms close-packed two-dimensional islands. The self-assembly is driven by stable hydrogen-bonded dimers with poor two-dimensional order. On Cu(111) complex structures are observed exhibiting, in addition, a strong annealing temperature dependence. We determine the corresponding structural transformations to be driven by gradual deprotonation of the uracil molecules. Our XPS study reveals unambiguously the tautomeric signature of uracil in the contact layer and on Cu(111) the molecule's deprotonation sites. The metal-mediated deprotonation of uracil and the subsequent electron localization in the molecule determine important biological reactions. Our data show a dependence between molecular coverage and molecule–metal interaction on Cu(111), as the molecules tilt at higher coverages in order to accommodate a higher packing density. After deprotonation of both uracil N atoms, we observe an adsorption geometry that can be understood as coordinative anchoring with a significant charge redistribution in the molecule. DFT calculations are employed to analyze the surface bonding and accurately describe the pertaining electronic structure.

Keywords: uracil, copper surface, silver surface, scanning tunneling microscopy, X-ray photoelectron spectroscopy, near-edge X-ray absorption fine structure, density functional theory

Uracil (Figure 1) is an RNA base, in particular the base differentiating RNA from DNA, and as such plays a vital role in biological interactions of major importance, notably those governing information transport and catalytic functions. Historically, uracil has been employed in the 1961 illustrious experiment of Nirenberg and Matthaei,[1] which demonstrated that polyuridylic acid translates into a protein of poly-L-phenylalanine, functioning as a synthetic template or mRNA and therefore cracking the first genetic codon, UUU. Currently, the advance of RNA deciphering has shown that, together with adenine, uracil is a part of all three stop codons.

The surface adsorption and self-assembly of the fundamental building blocks of the genetic code and especially of the nucleobases have been the subject of intensive investigations in the last decades. There is a twofold aspect in these works. One part focuses on gaining a fundamental understanding of biological reactions on surfaces. For instance, the adsorption of biological molecules on inorganic solids is regarded as a relevant prebiotic process, and it is considered to be related to the origin of life.[2]

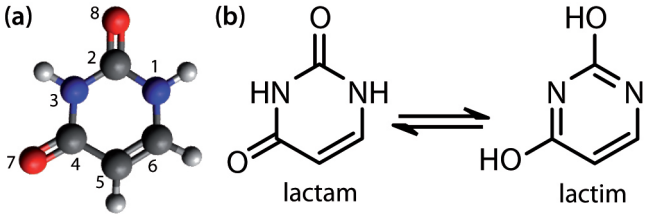

FIG. 1. Uracil: (a) 3D ball-and-stick model in its canonical form showing the labeling convention for the constituent atoms and (b) molecular structure highlighting the lactam and lactim tautomers, the most commonly observed uracil tautomers in nature.

Also, insight into the behavior of these building blocks similarly provides potential in biomimetic applications. Nature is extremely successful in performing tasks such as information storage, transfer, and catalysis by using these building blocks. Hence in the emerging field of nanotechnology, which focuses on the interactions between nanoscale moieties,[3,4] biomimetic applications have been proposed for performing the same tasks.[5,6]

The unique chemical functionalities of nucleobases offer a plethora of possible applications: their potential for

[a)] Electronic mail: a.c.papageorgiou@tum.de

[b)] Electronic mail: joachim.reichert@tum.de

chiral recognition on surfaces, an important target of the fine chemical industry, was shown by the elegant work of Chen and Richardson, who visualized the enantiomeric interaction between adenine and phenylglycine on the Cu(110) surface.[7] In the field of surface nanoarchitectonics they have been used as monomers or moieties, which offer multiple sites for hydrogen bonding, in binary and ternary supramoecular networks.[8−10] Additionally DNA bases offer the possibility of metal ligand interactions,[11] thus of engineering metal–organic networks.[12,13] Their attractiveness is obvious, being inexpensive, nontoxic, and biocompatible. However, in order to harness their full potential in such applications, it is vital to be able to predict their chemical reactivity toward the employed templates, which include close-packed coinage metals, TiO_2, and graphite.

These reasons have spurred numerous studies on the adsorption of nucleobases. It is beyond the scope of this paper to give a full literature overview; however our findings are discussed alongside previous work on uracil and the related DNA base, the 5-methyluracil, thymine. Briefly, uracil was studied by scanning tunneling microscopy (STM) on MoS_2, where it assembles into islands with clearly distinguished dimers, which do not correlate to the uracil single-crystal structure.[14,15] On the more inert support graphite, STM showed a structure that bears a close resemblance to the single crystal.[14−16] On Cu(111), trimeric units form at low surface coverage, whereas at higher surface coverage two-dimensional domains form, which were also modeled with a trimeric motif.[17] All the above studies assumed adsorption of uracil in its lactam form. However, vibrational spectroscopy revealed that uracil on Si(100)-2×1 adsorbs in its lactim form and interacts with the surface by cleavage of the O–H bond.[18] On Cu(110) photoelectron diffraction (PhD) coupled with X-ray photoelectron spectroscopy (XPS) and near-edge X-ray absorption fine structure (NEXAFS) indicated that N–H cleavage allows coordination to the surface with both O atoms and the N atom (N3) in between.[19] Finally, on Au(100),[20−22] Au(111),[21] and Ag(111),[23] cyclic voltammetry experiments showed uracil to switch from physisorbed to chemisorbed state.

Despite this extensive volume of work, there is a lack of multitechnique studies to unravel the fine interplay of uracil's functional units with the underlying substrate, which determines the molecules' chemical state, bonding configuration, and the resulting self-assembly scenario. Here we present a comprehensive study of uracil on Ag(111) and Cu(111). Silver and copper were chosen as commonly employed templates for molecular self-assembly and engineering of biomolecular nanostructures confined in two dimensions. Our approach includes experimental investigations combining STM, XPS, and NEXAFS coupled with density functional theory (DFT) simulations to elucidate the surface bonding and the charge transfer between the surface and the molecule as well as intramolecular electronic changes. Structural aspects were characterized at the molecular level by STM, revealing exquisite details of an intricate self-assembly scenario on Cu(111), which could be understood only by the complementary spectroscopic investigations and first-principles modeling using DFT. In particular, we found that the nanostructures formed are decisively influenced by specific interactions of uracil functional groups with the metal surface driving chemical transformations, which were previously unknown.

RESULTS AND DISCUSSION

Uracil on Ag(111).

As a model system, where intermolecular interactions prevail in the molecular surface organization, we investigated the system uracil on Ag(111). Figure 2a shows a typical STM image corresponding to uracil in contact with the hexagonal substrate. It is characterized by a uniformly packed structure. The close-packed islands are furnishing areas adjacent to step edges, without completely wetting the step edge. This is somewhat different from the observation of monolayer growth of uracil on Au(111), where the molecules form one-dimensional filaments at low coverages, but as the coverage increases toward the saturated monolayer, close-packed two-dimensional islands form.[8] On Ag(111) we find similar close-packed islands at uracil coverages as low as 0.3 ML, with 1 ML (monolayer) being defined as 100% of metal surface covered by the adsorbate. The molecule-to-molecule distances are measured to be within the range of 7–9 Å, consistent with flat-lying hydrogen-bonded molecules. The self-assembled layer has a loose connection to the substrate high-symmetry axes, but the broad spots of the fast Fourier transform (FFT) STM image in the inset of Figure 2a indicate that the registry of uracil to the Ag surface is not perfectly regular and therefore suggest an intermolecular interaction-driven pattern formation. As it was pointed out in a theoretical study of the 10 uracil homopairing possibilities, the energetically most favorable two-dimensional assemblies are not necessarily formed using only the most stable pairs, but other potential pairs may also be involved to accommodate additional bonding between nearest molecules.[24] For instance, the same authors found that the 21 possible adenine hydrogen-bonded homopairs can result in thousands of possible monolayer structures, many of which have similar lattice vectors.[24,25] So it comes as no surprise that in a system with a very weak interaction between surface and molecule, where the surface acts mainly to confine the overlayer in two dimensions and not as a strict directorial template, there is poor long-range ordering of the resulting overlayer. An illustration of these observations can be seen in Figure 2: although a model similar to the one proposed for uracil on graphite[16] can be fitted in small regions (Figure 2c), the structure exhibits frequent irregularities, as indicated by the red marks.

Further XPS and NEXAFS characterization of this

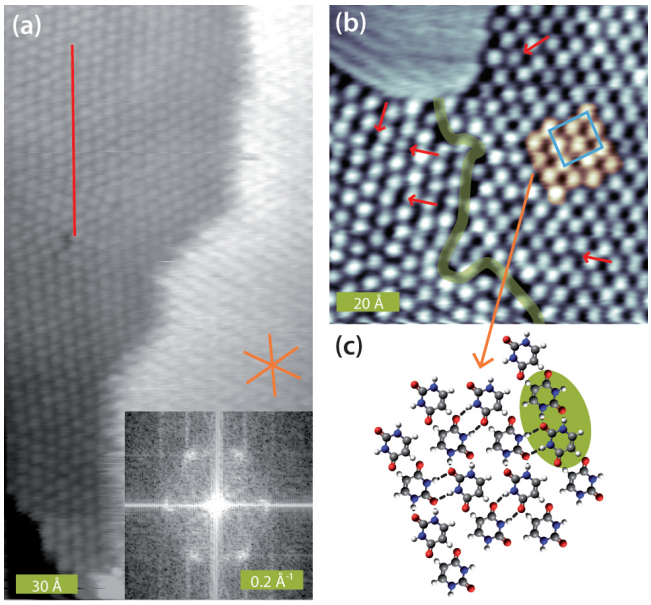

FIG. 2. STM images of ∼ 0.3 ML of uracil on Ag(111): (a) overview (I_t = 0.12 nA, V_t = 630 mV); inset shows the corresponding FFT; (b) detail with single-molecule resolution (I_t = 0.11 nA, V_t = 630 mV) showing a boundary of two domains (green thick line) and the unit cell of the overlayer structure (in blue); (c) tentative molecular model based on the most stable uracil homopairs (highlighted in green) for the orange highlighted area in (b). Red marks and arrows indicate deviations from the molecular model proposed in (c), and the Ag(111) high-symmetry axes are indicated in orange.

system confirms our interpretation of the STM data. Figure 3 summarizes the C 1s, N 1s, and O 1s XP spectra of uracil adsorbed in the temperature range of 300 to 330 K on Ag(111) and Cu(111). The central row shows the XP spectra corresponding to a monolayer of uracil on Ag(111). In the C 1s region we distinguish four clear peaks corresponding to the four carbon atoms of uracil, namely, in order of increasing binding energy, the atoms C5, C6, C4, and C2 (for the labeling of the uracil atoms see Figure 1a).[26] The N 1s region is characterized by a single peak (fwhm ∼ 1.3 eV) centered at a binding energy of 400.8±0.1 eV. The O 1s core level also appears as a single broad peak at a binding energy of 532.0 ± 0.1 eV with fwhm of 1.5 eV, in good accord with amide.[27] Comparing the spectra with the corresponding ones of the multilayer of physisorbed uracil (Figure 3 top spectra), it becomes evident that adsorption leads to an almost rigid shift of all six peaks by −0.5 eV. This shift is attributed to a polarization screening by the substrate and is typical for intact organic species on a metal substrate.[28] The uniformity of the shift is consistent with planar adsorption geometry with moderate metal–molecule interactions suggested by our STM data. In the multilayer regime, it is known that uracil is intact and in its canonical form, *i.e.*, as the lactam tautomer;[29] thus the same conclusion holds for the present system: uracil adsorbs intact as a lactam species at the Ag(111) vacuum interface.

Figure 4a shows C K-edge NEXAFS data of 1 ML of uracil on Ag(111) at 300 K recorded at three photon incidence angles θ (defined relative to the surface plane; see Supporting Information, Figure S1). The first four sharp resonances **A** to **D** correspond to transitions from C 1s to each of the first two available π^* orbitals, respectively. Resonance **E** exhibits an angular dependence following the π^* transitions; however it appears in a region where transitions cannot be clearly distinguished; two broad σ^* resonances **F** and **G** occur beyond the step edge of ionization (Figure 4a, gray dashed lines). A summary of the assignments and associated transitions is given in the Supporting Information (Table S1), based on the comparison with simulated NEXAFS[30] of the gas phase uracil molecule and experimental NEXAFS[29] of condensed uracil. As expected, both groups of π^* and σ^* resonances display distinct dichroism in their angular dependence.

Since the C atoms are approximately coplanar, the angular dependences observed in the C K-edge spectra provide a powerful means of determining the orientation of uracil with respect to the surface. Figure 4b presents such an analysis for the principal π^* resonances **A** to **D**, the observed normalized intensities being overlaid with a best-fit theoretical curve (solid gray line) for the molecular tilt angle (α) with respect to the surface. (In principle, σ^* resonances may be subject to a similar analysis, but their larger width and the fact that they are superimposed on the step background preclude accurate fitting.) The normalized intensities of the π^* resonances fit very consistently a uracil tilt angle of 10°±10°, indicating that the molecule is lying almost flat on the surface (Figure 4c).

The findings of this spectroscopic study are in line with the interpretation of our microscopy data. Perhaps the only discrepancy with earlier STM studies of uracil on inert surfaces, such as Ag(111),[23] Au(111),[21] and graphite,[16] is that in this work at room temperature we find poor long-range order, with relatively small patches of different two-dimensional networks. This could either arise from differences in experimental conditions, as the present work was carried out under ultrahigh vacuum rather than at the solid–liquid interface, or be a consequence of the local nature of the STM technique, which samples a minute surface area.

Uracil on Cu(111).

The following section is split into three parts: The first two describe the experimentally observed chemical modifications of uracil in different temperature regimes, as it will be revealed by the subsequent XP spectra; the third addresses the aforementioned chemical modifications with *ab initio* calculations.

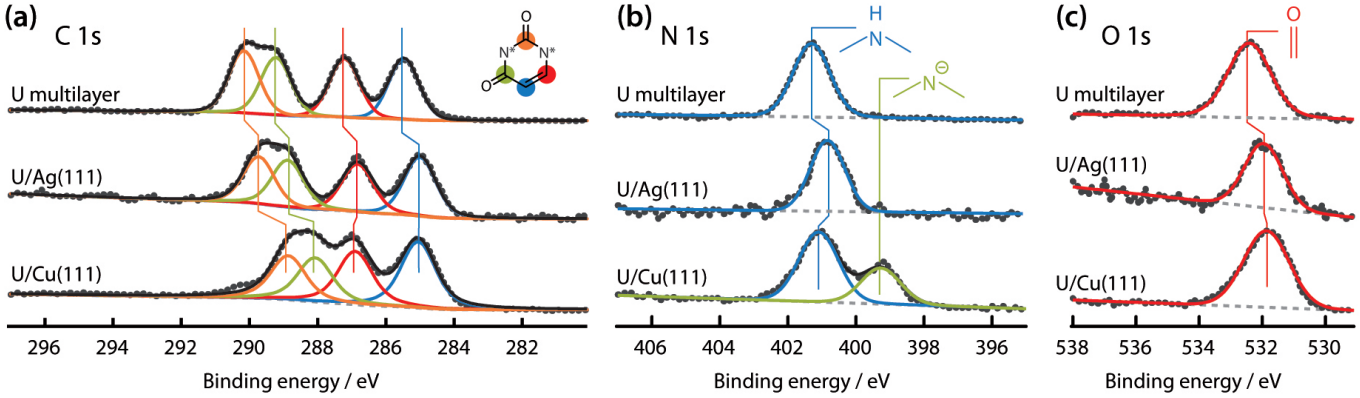

FIG. 3. Uracil XP spectra corresponding to a multilayer formed at 300 K (top), a saturated monolayer on Ag(111) formed at 330 K (middle), and a saturated monolayer on Cu(111) formed at 320 K (bottom) for the (a) C 1s, (b) N 1s, and (c) O 1s core levels.

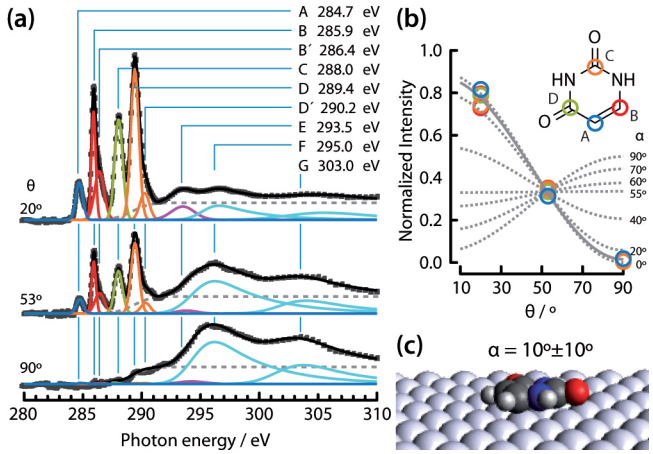

FIG. 4. (a) Experimental C K-edge NEXAFS data acquired at three angles of photon incidence, θ, for the 1 ML coverage of uracil on Ag(111) and respective fit analysis. (b) Curve-fitting analysis of the photon angle dependence of π^* resonances **A** to **D** to estimate the corresponding molecule tilt angle, α. (c) Illustration of adsorption geometry of uracil in the monolayer on Ag(111): the molecule tilt angle with respect to the surface is $\sim 10°$.

From 300 to 360 K.

On the Cu(111)surface,structures completely unrelated to those formed on Ag(111) appear in the first layer. Deposition of $\sim$ 0.3 to 0.8 ML of uracil at room temperature on Cu(111) yielded a surface with a mixture of two phases, a "tiare" (Figure 5) and a "zigzag" (Figure 6) pattern imaged by STM at room temperature. We will describe the self-assembly of these phases before we proceed with the description of their dynamical interchange.

The tiare phase is a commensurate phase, as evidenced by the lack of any moir pattern, and its rhombic unit cell (Figure 5a) can be described in Wood's notation by a $9(\sqrt{3} \times \sqrt{3})R30°$ overlayer. This means that on the (111) surface there is only one symmetry domain. However, this is an intrinsically chiral phase, as evidenced by the S and R "petal" orientation of the tiare motif (Figure 5b–d). As such, it is a rare example of a nondensely packed two-dimensional chiral phase of a nucleobase, other reported examples being guanine/ Au(111)[31] and xanthine/Au(111).[32] In the center of the tiare motif and in between the petals, features of high contrast are commonly observed (Figure 5c), which we attribute to weakly bound diffusing molecules trapped in the tiare nanocages. The tiare phase was observed in an earlier study of uracil on Cu(111) at $\sim$ 77 K and described as "snow-crystal-like",[17] because in those STM images the chirality could not be resolved. Besides achieving better resolution, in our images we can resolve 30 distinct bright protrusions per unit cell, as opposed to 18 in the previous study.[17] Each tiare flower consists of six pentamer petals. In that earlier study it was concluded that the bright protrusions correspond to single, intact molecules, their round shape and apparent height indicating flat-lying molecules and their separation being consistent with hydrogen bonding. However, the proposed model[17] cannot be substantiated if we assume 30 intact, flat-lying molecules per unit cell: the resulting molecular distances are, in fact, too small for such a model to be consistent.

In the zigzag phase the molecular density is even higher, the bright protrusions having oblong shapes. This suggests tilted molecules, which interact strongly with the underlying substrate. To understand the mixture of the phases, we performed temperature- and coverage-dependent STM measurements. We found that the balance of the mixture is shifted with heating this surface to just 320 K: only the tiare phase is observed. The opposite effect in this balance comes from increasing the coverage to a saturated monolayer: only the zigzag phase was present after the preparation of a saturated monolayer. This implies that both of these phases must be made of the same molecular unit.

To identify this unit, we looked at the 1s core level

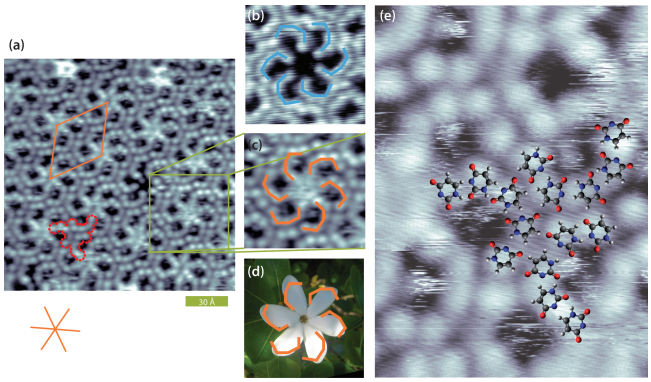

FIG. 5. (a) STM image of submonolayer coverage of uracil on Cu(111) at $\sim$ 300 K showing a domain of the tiare phase ($I_t = 0.13$ nA, $V_t = 1201$ mV). The Cu(111) high-symmetry axes and the superstructures' unit cell are indicated in orange. (b) Tiare motif in STM images of an *S*-petalled domain ($I_t = 0.11$ nA, $V_t = 857$ mV) and (c) that of an *R*-petalled domain, indicated by the green square in (a) ($I_t = 0.13$ nA, $V_t = 1201$ mV). (d) For comparison a photograph of an *R*-petalled tiare flower. (e) Tentative model of tiare phase, corresponding to an area indicated by the red dotted line in (a), overlaid on the STM image ($I_t = 0.13$ nA, $V_t = 1201$ mV).

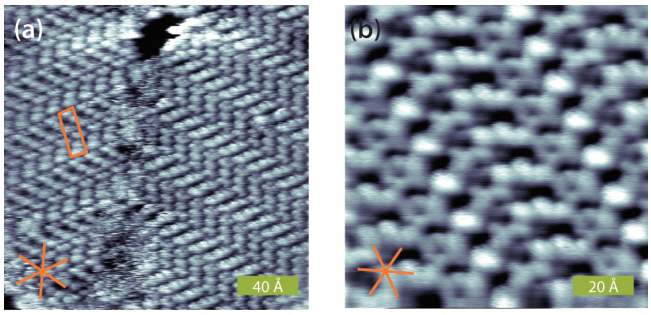

FIG. 6. STM images of the "zigzag" phase of uracil on Cu(111) at $\sim$ 300 K showing (a) overview ($I_t = 0.11$ nA, $V_t = 857$ mV) and (b) detail ($I_t = 0.13$ nA, $V_t = 1250$ mV). The Cu(111) high-symmetry axes and the superstructures' unit cell are indicated in orange.

binding energies of the distinct atoms of our molecule as done before. These are displayed in the bottom row of spectra in Figure 3, and we find marked differences relative to the case of the Ag(111) substrate. Most prominent is the appearance of a new, additional peak in the N 1s level shifted in binding energy by ~ -2 eV with respect to that of the intact protonated nitrogen. We assign it to deprotonation of a single uracil nitrogen. This proton is not recaptured by the molecule: The O 1s core level does not show any significant change when compared to the multilayer of uracil, apart from the shift associated with the metal surface interaction. Furthermore, by close inspection of the C 1s core level we can identify the deprotonated N atom. The peaks originating from atoms C5 and C6 (cf. Figure 1a, marked in Figure 3 by blue and red, respectively) are unaffected by the chemical transformation of the molecule, whereas peaks C4 and C2 (marked in Figure 3 by green and orange, respectively) are both shifted downward by $\sim$ 1 eV, reflecting the rearrangement of electron distribution after the chemical change in the nearest neighboring N atom. Had it been a deprotonation of the N1 site, the chemical shift would be observed in the peaks corresponding to C2 and C6 atoms. Consequently, it is the N3 atom that undergoes deprotonation, as it is also the case for uracil and the closely related species, thymine, on the Cu(110) surface[19,33] and in solution,[34] but not in the gas phase, where the N1 atom is found to be more acidic.[35] However the authors of the last study argue also that the stability of $N3^-$ is enhanced in polar solvents, therefore tuning the deprotonation selectivity in a biological environment. Our study shows that in the case of metal-mediated deprotonation, it is the N3 site that undergoes preferential deprotonation.

From the previous considerations, it is clear that the tiare phase described above bears a nontrivial interaction with the underlying substrate: it consists of uracil molecules with the N3 atom deprotonated, and hence we need to establish an atomistic structural model of this phase. Given that the STM indeed shows roundish protrusions, similar in shape to uracil/Ag(111), we can assume flat-lying molecules and tentatively propose the model shown in Figure 5e. It is a structure consisting of homochiral pentamer "petals", repeated with 6-fold symmetry (as dictated by the substrate symmetry) to generate a "tiare" motif. The resulting molecular structure is stabilized by hydrogen bonding, N–H$\cdots$O=C, and additional lateral interactions involving, N^-, C–H, and C=O groups at the pentamer and C–H and C=O moieties between neighboring pentamers. Uracil is an achiral molecule in the gas phase; however its reduced symmetry turns it into chiral once confined on a two-dimensional plane. It is noteworthy that in the model proposed above the two chiral domains consist of enantiopure uracil monomers deprotonated at N3.

The STM images of the zigzag phase, on the other hand, suggest a strongly tilted molecule. Indeed, this is in accordance with NEXAFS measurements on the saturated monolayer, which consists only of this phase. Figure 7a shows the corresponding NEXAFS data at three angles of photon incidence. The resonances observed are assigned in the Supporting Information (Table S2). Using the same curve-fitting analysis procedure as for uracil on Ag(111), which provides the photon angle dependence of π^* resonances **A** to **D** (Figure 7b), we estimate the molecule tilt angle of the zigzag phase to be $\sim 65°$ (Figure 7c).

By close inspection of the zigzag phase we find that the longer axis of the molecular elliptical shapes aligns along the high-symmetry axes. This is consistent with PhD measurements, a powerful technique for accurate determination of the adsorbate geometry, of uracil and the similar DNA base, thymine, on Cu(110).[19,33] Both molecules are found to bind along the close-packed direc-

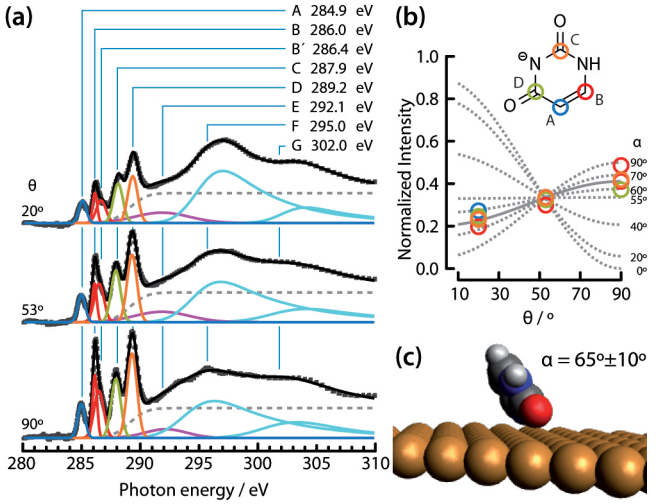

FIG. 7. (a) Experimental C K-edge NEXAFS data acquired at three angles of photon incidence, θ, for the 1 ML coverage of uracil on Cu(111) and respective fit analysis. (b) Curve-fitting analysis of the photon angle dependence of π^* resonances **A** to **D** to estimate the corresponding molecule tilt angle, α. (c) Illustration of adsorption geometry of uracil in the monolayer on Cu(111): the molecule tilt angle with respect to the surface is $\sim 65°$.

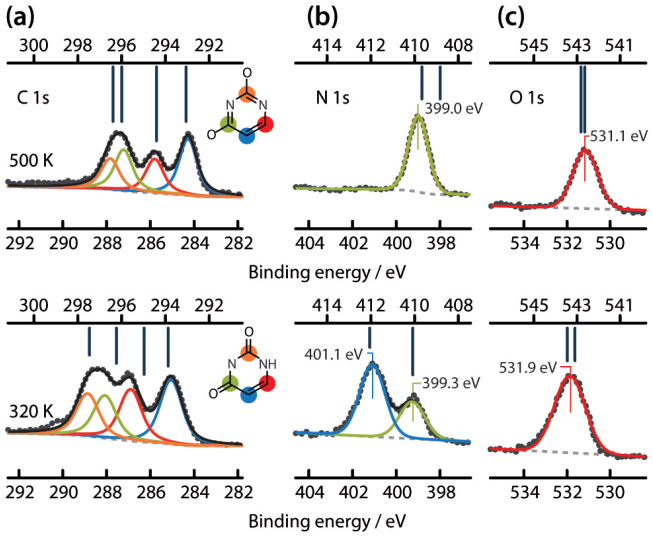

FIG. 8. Uracil XP spectra of (a) C 1s, (b) N 1s, and (c) O 1s core levels corresponding to a saturated monolayer on Cu(111) formed at 320 K (lower spectra) and after heating the surface to 500 K (top spectra). Solid lines on top of spectra mark the calculated binding energies of the core levels corresponding to the two configurations of singly (320 K) and doubly (500 K) deprotonated uracil on Cu(111).

tion of Cu. The close match of the O–N^-–O projected distances presumably drives the binding to the Cu atoms of the close-packed rows along the $< 1\bar{1}0 >$ direction. Figure 6b reveals also features of different contrast in STM data; therefore it is plausible that molecules with different adsorption geometries are present. From the NEXAFS measurements we deduce the average tilt of the molecular ensemble to be $\sim 65°$; therefore, we can conclude that this phase consists *mainly* of strongly inclined molecules.

At the temperature of formation the presence of diffusing Cu adatoms is known to play an important role in the deprotonation and surface coordination of compounds with carboxylic acid moieties[36,37] and in the surface coordination and adsorption of compounds containing pyridyl groups.[38–40] In the phases described above there is no direct evidence for their involvement in the structure. In the tiare phase the intermolecular distance is too short to allow the incorporation of metal adatoms. In the zigzag phase, the molecules have a high tilt angle, allowing uracil molecules to coordinate with both oxygen atoms and the deprotonated N3 toward the surface, as also supported by the DFT results presented below. However, it is possible that undercoordinated adatoms are important in activating the N–H scission observed.[41]

From 400 to 550 K.

Heating the uracil monolayer on Cu(111) to higher temperatures and monitoring the N 1s signal (Figure 8b), one can primarily observe the increase of the deprotonated N signal along with a concomitant decrease in the molecular coverage (Supporting Information, Figure S2). By 500 K only deprotonated N is present, while a shift of -0.8 eV is observed in the O 1s signal (Figure 8c) and the C 1s shows a significant charge redistribution (Figure 8a). Clearly, the uracil molecules after this heat treatment are doubly deprotonated. Our spectroscopy data are again comparable to the case of uracil on Cu(110).[19]

However, unlike the topography of uracil on Cu(110) after annealing to 400 K,[42] no adsorption-induced surface faceting was observed on Cu(111). The corresponding topography observed in our STM investigation is shown in Figure 9. Trilobed structures, oriented along the $< \bar{2}11 >$ direction of Cu(111), appear among less ordered mobile molecules and are stable on the surface after heating in the range from 400 to 550 K. In the trilobed structures (Figure 9b) elliptically shaped protrusions corresponding to the lateral dimensions of tilted single molecules are discernible. Their separation along the $[\bar{2}11]$ Cu(111) direction is $\sim 4.5-4.7$ Å, whereas that along the close-packed [110] is ~ 6 Å, supporting that the trilobed structures consist of tilted molecules in a similar local adsorption geometry to that in the zigzag phase (Figure 6b).

Indeed the corresponding angular dependence of NEXAFS reveals an average tilt angle of $\sim 60°$ (see Supporting Information Figure S3). However it is striking that the doubly deprotonated uracil forms close-packed structures, such as the ones of the trilobe. Intuitively, we can rationalize the formation of such dense packing with charge transfer from the substrate metal. But having a tilted uracil molecule means that both N atoms cannot

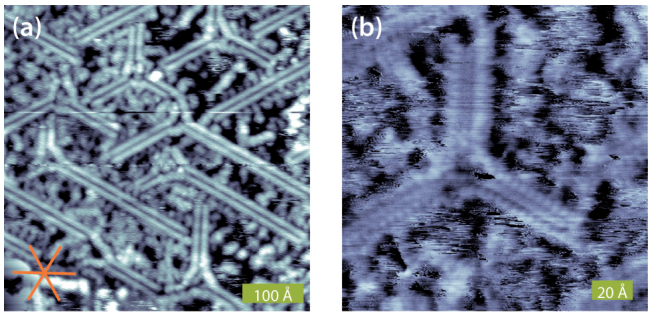

FIG. 9. STM images of 1 ML of the trilobed structure (uracil on Cu(111) after heating to 500 K): (a) overview (I_t = 0.29 nA, V_t = 2900 mV) and (b) detail (I_t = 0.14 nA, V_t = 1250 mV). The substrate high-symmetry axes are indicated in orange.

be in close contact with the metal surface. Hence most probably the electron charge is relocalized on the uracil O atoms, both of which can be in close contact with the surface.

DFT Modeling.

In order to get deeper insight into the uracil surface chemical bonding and electronic structure, we performed DFT calculations of singly and doubly deprotonated single uracil molecules on Cu(111). From these, the binding energies of the C 1s, N 1s, and O 1s core levels were computed and are displayed above the corresponding experimental spectra in Figure 8. The good agreement obtained in the relative shifts between experimentally measured and theoretically calculated core levels allows us to be confident about the approximation of the ensemble of adsorbed uracil radical molecules with an isolated molecule and the current interpretation of the spectroscopy data.

Figure 10 shows the corresponding fully relaxed adsorption geometries superimposed on the electron density differences between the adsorbed molecule on the Cu(111) and the corresponding uracil radical and the pristine Cu(111) surface; for a one-dimensional charge difference averaged along the surface plane see Supporting Information Figure S4. As for the case of uracil[19] and thymine[33] on Cu(110), the deprotonated uracil is coordinatively anchored upright along the Cu closed-packed direction in a tridentate configuration. The smaller tilt angles derived by the NEXAFS analysis reported above originate presumably from the intermolecular interactions in the self-assembled structures and/or because of the coexistence of different local adsorption modes. The binding energies of these configurations are given by $E_{\mathrm{bind}} = -(E_{\mathrm{uracil/Cu}} - E_{\mathrm{uracil}} - E_{\mathrm{Cu}})$, where "uracil" here refers to the uracil radical, and are 3.433 and 4.438 eV for the singly and doubly deprotonated molecules, respectively. The electron density differences of the adsorbed uracil from the radical molecules (Figure 10) in both cases exhibit significant charge redistribution upon adsorption, with a gain of electrons (red regions) and loss of them (blue) in several regions. Moreover, the substrate atoms seem to gain negative charge in the d_{xz} and d_{yz} orbitals when the molecule is adsorbed and lose from the d_{z^2} orbitals. The Bader analysis gives a charge transfer of 0.6 electron to the molecules in the configuration shown in Figure 10a (deprotonated at N3) and 1.1 electrons in the configuration shown in Figure 10b (deprotonated at both N1 and N3).

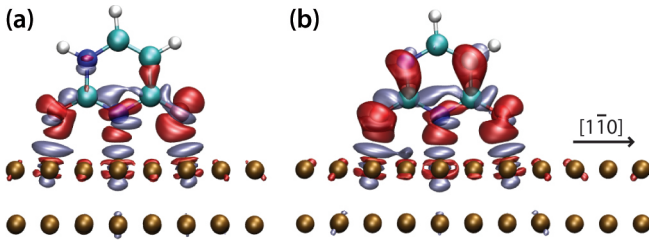

FIG. 10. Three-dimensional representation of the electron density differences of (a) a singly and (b) a doubly deprotonated uracil molecule on Cu(111) from the electron density of the corresponding uracil radical and the pristine Cu(111) surface. Red and blue regions indicate areas of gain and loss of electrons, respectively.

Such a scenario of electron charge shifting can actually help interpret earlier reflection absorption infrared spectroscopy (RAIRS) results of thymine on Cu(110),[43] which showed that the C=O vibrational mode disappeared after annealing at 558 K, indicative of the formation of strong bonds to surface atoms. The PhD study of the same system revealed that thymine preserves its tridentate adsorption geometry upon annealing and creates doubly deprotonated thymine molecules.33 Moreover, PhD investigations of both uracil and thymine on Cu(110) found the O–Cu distances to be comparable with the typical O–Cu distances of acetate species on the same surface, further supporting the formation of molecular bonds between O and Cu.[19,33]

Summary and Conclusions.

We have performed a detailed study of the first molecular layer of uracil on close-packed noble metal surfaces using state-of-the-art STM, synchrotron XPS, and NEXAFS coupled with DFT, which provides a deep understanding of these systems. We have found that on Ag(111) uracil adsorbs almost flat, intact, and forms a densely packed hydrogen-bonded network with poor long-range order. This is contrasted by the behavior on Cu(111), where uracil deprotonates at the N3 site upon adsorption at room temperature. Two different phases are revealed depending on the local density of uracil. A tiare phase, which prevails at low coverages where the presence of bare Cu patches facilitate molecular diffu-

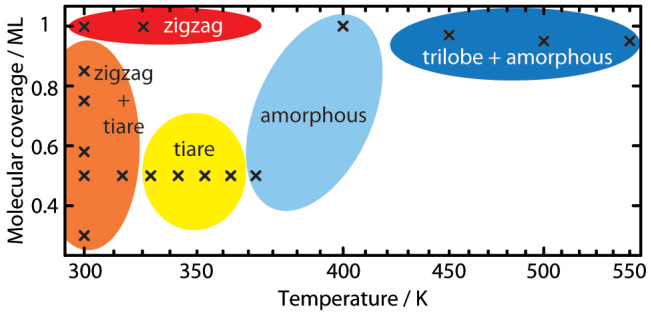

FIG. 11. Schematic overview of the overlayer structures formed by uracil on Cu(111) as a function of annealing temperature.

sion, consists of flat-lying monomers, thus maximizing the interaction of the π orbitals of the molecule with the metal surface. As the coverage increases, the molecule tilts with respect to the surface with an average tilt angle of $\sim 65°$, accommodating a more dense layer in contact with the Cu surface. By heating the saturated monolayer uracil film on Cu(111) to 500 K, also the N1 atom deprotonates, and a new type of trilobed nanostructure forms. A schematic overview of the overlayer structures found is depicted in Figure 11.

Similarly to the different behavior of methionine on Ag(111)[44] and on Cu(111),[45] we demonstrated the importantance of the subtle increase in substrate reactivity in tailoring the resulting nanoarchitectures. Among the phases formed, we observed a tiare phase forming chiral nanocages, which additionally feature reactive sites in their inner periphery, thus making this phase suitable for exploitation as a molecular recognition template. Finally, we addressed the gradual deprotonation of the uracil N atoms and the occurring charge redistribution within the molecule, providing a coherent description of the uracil interaction with the metal surface. These chemical transformations are of relevance in the biological environments, tuning the interaction selectivity of particular sites of uracil.

METHODS

STM experiments were conducted in Garching in a home-made UHV chamber equipped with an Aarhus-type variable-temperature STM, which was operated in constant-current mode using chemically etched tungsten tips. STM images were processed with WSxM.[46] All lateral dimensions reported are within an accuracy of <10%.

Synchrotron XPS and NEXAFS measurements were carried out at the HE-SGM monochromator dipole magnet beamline at the BESSY II synchrotron radiation source in Berlin, which provides light with a linear polarization of 90%. Spectra were collected using a Scienta R3000 electron energy analyzer. The angle between the analyzer entrance lens and the incoming photon beam was 45° in the horizontal plane. To ensure that our measurements were not compromised by molecular beam damage, as it has been reported for this kind of molecule,[47] we performed our measurements in low-alpha operation mode (beam current after injection 15 to 40 mA *vs* 300 mA in normal-mode operation). The absence of beam damage was further confirmed by monitoring the consistency of the data.

For the NEXAFS measurements at the C K-edge, N K-edge, and O K-edge the partial electron yield mode of detection (retarding voltages of 150, 250, and 450 V, respectively) was used. All spectra were recorded at $\sim$ 300 K and referenced against a characteristic peak in simultaneously recorded spectra of a contaminated Au grid. Spectra at each angle of incidence represent an average of three to five spectra. Following a standard procedure, we processed the raw data by subtracting the signal of the bare crystal, then correcting for the transmission through the beamline, and finally normalizing the edge jump to 1.

The excitation energies used for the acquisition of the N 1s, O 1s, and C 1s spectra were 550, 680, and 435 eV, respectively. Photoelectron spectra were recorded in normal emission. The binding energy scale of the XP spectra was calibrated against the Ag $3d_{5/2}$ line at 368.3 eV for the multilayer uracil film and the uracil on Ag(111) data and against the Cu $3p_{3/2}$ line at 75.1 eV for uracil on Cu(111). For the XPS data fitting a Shirley plus linear background was subtracted from the raw data, and Voigt functions were used to fit the components. The width and shape of the Voigt functions used were kept fixed for a given core level at a given preparation.

The Ag(111) and Cu(111) surfaces were cleaned by repeated cycles of Ar^+ sputtering (99.999%, Linde) followed by annealing at 700 and 770 K, respectively, until clean, atomically flat surfaces were obtained, as monitored by XPS (Berlin) or STM (Garching). The temperature was monitored by T1T2 thermocouples (type K) directly attached to the single crystals. Uracil ($\geq$99%, Sigma) was dosed onto the samples by means of an organic molecular beam epitaxy source (vacuum sublimation temperature of 420–470 K).

We performed DFT calculations using both the generalized gradient approximation (GGA) of Perdew, Burke, and Ernzerhof[48] and the van der Waals density functional (vdW-DF2)[49] accompanied with the C09 exchange functional.[50] Since the two methods yielded very similar results, we show only the results from the GGA calculations. We modeled the system within the slab geometry of a laterally rectangular $c(5 \times 8)$ cell to isolate the molecule from its periodic images and four layers of substrate, of which the two uppermost were fully relaxed. A dipole correction was used to correct for the different asymptotic potentials at the different sides of the slab. A 2×2 mesh of k points was used to integrate over the Brillouin zone and Fermi-Dirac broadening of the occupation numbers around the Fermi energy with a width sigma = 0.05 eV; the energies were subsequently extrapolated to

zero temperature. We used plane-wave expansion for the wave functions in plane waves employing the Quantum ESPRESSO code[51] with ultrasoft pseudopotentials[52] to relax and analyze the system and Vienna Ab-initio Simulation Package (VASP)[53] with the projector-augmented method[54] for the core level binding energies, removing half of an electron from the core level and calculating the energetic distance's Kohn–Sham eigenvalue from the Fermi energy. The approximations led to an error, which we expect to be, however, systematic and constant for a given element.

ACKNOWLEDGMENTS

The authors thank Michael Naboka for technical assistance during the synchrotron experiments, and Alexei Nefedov and Christof Wöll for kindly providing access to the HE-SGM end station. This work was performed under the aegis of the EU FP7 program through the European Research Council Advanced Grant MolArt (no. 247299) and the Marie Curie Intra-European Fellowship NASUMECA (no. 274842).

Supporting Information Available:

Schematic of NEXAFS setup; C K-Edge NEXAFS peak assignments of 1 ML uracil on Ag(111) and on Cu(111); XP spectra of 1 ML uracil on Cu(111) as a function of annealing temperature; C K-edge NEXAFS data and analysis for the 1 ML coverage of uracil on Cu(111) formed at 320 K and postannealed to 500 K; 1D representation of the electron density differences averaged over the planes along the surface of a singly and a doubly deprotonated uracil molecule on Cu(111) from the electron density of the corresponding uracil radical and the pristine Cu(111) surface. This material is available free of charge via the Internet at http:// pubs.acs.org.

REFERENCES AND NOTES

1. Nirenberg, M. W.; Matthaei, J. H. The Dependence of Cell-free Protein Synthesis in E. Coli upon Naturally Occurring or Synthetic Polyribonucleotides. *Proc. Natl. Acad. Sci. U. S. A.* **1961**, *47*, 1588–1602.

2. Sowerby, S. J.; Cohn, C. A.; Heckl, W. M.; Holm, N. G. Differential Adsorption of Nucleic Acid Bases: Relevance to the Origin of Life. *Proc. Natl. Acad. Sci. U. S. A.* **2001**, *98*, 820–822.

3. Klappenberger, F.; Kühne, D.; Krenner, W.; Silanes, I.; Arnau, A.; García de Abajo, F. J.; Klyatskaya, S.; Ruben, M.; Barth, J. V. Dichotomous Array of Chiral Quantum Corrals by a Self-Assembled Nanoporous Kagomé Network. *Nano Lett.* **2009**, *9*, 3509–1514.

4. Schiffrin, A.; Reichert, J.; Auwärter, W.; Jahnz, G.; Pennec, Y.; Weber-Bargioni, A.; Stepanyuk, V. S.; Niebergall, L.; Bruno, P.; Barth, J. V. Self-Aligning Atomic Strings in Surface-Supported Biomolecular Gratings. *Phys. Rev. B* **2008**, *78*, 035424.

5. Sowerby, S. J.; Holm, N. G.; Petersen, G. B. Origins of Life: a Route to Nanotechnology. *Biosystems* **2001**, *61*, 69–78.

6. Mann, S. Life as a Nanoscale Phenomenon. *Angew. Chem., Int. Ed.* **2008**, *47*, 5306–5320.

7. Chen, Q.; Richardson, N. V. Enantiomeric Interactions between Nucleic Acid Bases and Amino Acids on Solid Surfaces. *Nat. Mater.* **2003**, *2*, 324–328.

8. Gardener, J. A.; Shvarova, O. Y.; Briggs, G. A. D.; Castell, M. R. Intricate Hydrogen-Bonded Networks: Binary and Ternary Combinations of Uracil, PTCDI, and Melamine. *J. Phys. Chem. C* **2010**, *114*, 5859–5866.

9. Palma, C.-A.; Bjork, J.; Bonini, M.; Dyer, M. S.; Llanes-Pallas, A.; Bonifazi, D.; Persson, M.; Samorì, P. Tailoring Bicomponent Supramolecular Nanoporous Networks: Phase Segregation, Polymorphism, and Glasses at the Solid–Liquid Interface. *J. Am. Chem. Soc.* **2009**, *131*, 13062–13071.

10. Llanes-Pallas, A.; Matena, M.; Jung, T.; Prato, M.; Stöhr, M.; Bonifazi, D. Trimodular Engineering of Linear Supramolecular Miniatures on Ag(111) Surfaces Controlled by Complementary Triple Hydrogen Bonds. *Angew. Chem., Int. Ed.* **2008**, *47*, 7726–7730.

11. Barth, J. V. Fresh Perspectives for Surface Coordination Chemistry. *Surf. Sci.* **2009**, *603*, 1533–1541.

12. Xu, W.; Wang, J.; Yu, M.; Lægsgaard, E.; Stensgaard, I.; Linderoth, T. R.; Hammer, B.; Wang, C.; Besenbacher, F. Guanine- and Potassium-Based Two-Dimensional Coordination Network Self-Assembled on Au(111). *J. Am. Chem. Soc.* **2010**, *132*, 15927–15929.

13. Purohit, C. S.; Verma, S. Patterned Deposition of a Mixed- Coordination Adenine–Silver Helicate, Containing a π-Stacked Metallacycle, on a Graphite Surface. *J. Am. Chem. Soc.* **2007**, *129*, 3488–3489.

14. Sowerby, S. J.; Petersen, G. B. Scanning Tunneling Microscopy of Uracil Monolayers Self-assembled at the Solid|Liquid Interface. *J. Electroanal. Chem.* **1997**, *433*, 85–90.

15. Sowerby, J. S.; Edelwirth, M.; Heckl, W. M. Molecular Mechanics Simulation of Uracil Adlayers on Molybdenum Disulfide and Graphite Surfaces. *Appl. Phys. A: Mater. Sci. Process.* **1998**, *66*, S649–S653.

16. Mamdouh, W.; Kelly, R. E. A.; Dong, M.; Kantorovich, L. N.; Besenbacher, F. Two-Dimensional Supramolecular Nanopatterns Formed by the Coadsorption of Guanine and Uracil at the Liquid/Solid Interface. *J. Am. Chem. Soc.* **2008**, *130*, 695–702.

17. Nakagawa, T.; Tanaka, H.; Kawai, T. Two-dimensional Self-Assembly of Uracil Molecules on Cu(111) Surfaces: A Low-Temperature STM Study. *Surf. Sci.* **1997**, *370*, L144– L148.

18. Lopez, A.; Chen, Q.; Richardson, N. V. Combined STM, HREELS and *ab Initio* Study of the Adsorption of Uracil on Si(100)-2×1. *Surf. Interface Anal.* **2002**, *33*, 441–446.

19. Duncan, D. A.; Unterberger, W.; Kreikemeyer-Lorenzo, D.; Woodruff, D. P. Uracil on Cu(110): A Quantitative Structure Determination by Energy-Scanned Photoelectron Diffraction. *J. Chem. Phys.* **2011**, *135*, 014704.

20. Dretschkow, Th.; Wandlowski, Th. In-Situ Scanning Tunneling Microscopy Study of Uracil on Au(100). *Electrochim. Acta* **1998**, *43*, 2991–3006.

21. Dretschkow, Th.; Dakkouri, A. S.; Wandlowski, Th. In-Situ Scanning Tunneling Microscopy Study of Uracil on Au(111) and Au(100). *Langmuir* **1997**, *13*, 2843–2856.

22. Irrera, S.; de Leeuw, N. H. A Density Functional Theory Study of the Adsorption of Uracil on the Au(100) surface. *Proc. R. Soc. A* **2011**, *467*, 1959–1969.

23. Cavallini, M.; Aloisi, G.; Bracali, M.; Guidelli, R. An in Situ STM Investigation of Uracil on Ag(111). *J. Electroanal. Chem.* **1998**, *444*, 75–81.

24. Kelly, R. E. A.; Kantorovich, L. N. Homopairing Possibilities of the DNA Base Thymine and the RNA Base Uracil: An ab Initio Density Functional Theory Study. *J. Phys. Chem. B* **2006**, *110*, 2249–2255.

25. Kelly, R. E. A.; Kantorovich, L. N. Hexagonal Adenine Net- works Constructed from their Homopairings. *Surf. Sci.* **2005**, *589*, 139–152.

26. Haug, A.; Schweizer, S.; Latteyer, F.; Casu, M. B.; Peisert, H.; Ochsenfeld, C.; Chassé, T. Thin-Film Properties of DNA and RNA Bases: A Combined Experimental and Theoretical Study. *ChemPhysChem* **2008**, *9*, 740–747.

27. Feyer, V.; Plekan, O.; Richter, R.; Coreno, M.; Vall-Ilosera, G.; Prince, K. C.; Trofimov, A. B.; Zaytseva, I. L.; Moskovskaya, T. E.; Gromov, E. V.; et al. Tautomerism in Cytosine and Uracil: An Experimental and Theoretical Core Level Spectroscopic Study. *J. Phys. Chem. A* **2009**, *113*, 5736–5742.

28. Chiang, T.-C.; Kaindl, G.; Mandel, T. Layer-resolved Shifts of Photoemission and Auger Spectra from Physisorbed Rare-Gas Multilayers. *Phys. Rev. B* **1986**, *33*, 695–711.

29. Zubavichus, Y.; Shaporenko, A.; Korolkov, V.; Grunze, M.; Zharnikov, M. X-ray Absorption Spectroscopy of the Nucleotide Bases at the Carbon, Nitrogen, and Oxygen K-Edges. *J. Phys. Chem. B* **2008**, *112*, 13711–13716.

30. Feyer, V.; Plekan, O.; Richter, R.; Coreno, M.; de Simone, M.; Prince, K. C.; Trofimov, A. B.; Zaytseva, I. L.; Schirmer, J. Tautomerism in Cytosine and Uracil: A Theoretical and Experimental X-ray Absorption and Resonant Auger Study. *J. Phys. Chem. A* **2010**, *114*, 10270–10276.

31. Otero, R.; Schöck, M.; Molina, L. M.; Lægsgaard, E.; Stensgaard, I.; Hammer, B.; Besenbacher, F. Guanine Quartet Networks Stabilized by Cooperative Hydrogen Bonds. *Angew. Chem., Int. Ed.* **2005**, *44*, 2270–2275.

32. Yu, M.; Wang, J.; Mura, M.; Meng, Q.; Xu, W.; Gersen, H.; Lægsgaard, E.; Stensgaard, I.; Kelly, R. E. A.; Kjems, J.; et al. Homochiral Xanthine Quintet Networks Self-Assembled on Au(111) Surfaces. *ACS Nano* **2011**, *5*, 6651–6660.

33. Allegretti, F.; Polcik, M.; Woodruff, D. P. Quantitative Determination of the Local Structure of Thymine on Cu(110) Using Scanned-Energy Mode Photoelectron Diffraction. *Surf. Sci.* **2007**, *601*, 3611–3622.

34. Thureau, P.; Ancian, B.; Viel, S.; Thévand, A. Determining Chemical Exchange Rates of the Uracil Labile Protons by NMR Diffusion Experiments. *Chem. Commun.* **2006**, 200–202.

35. Kurinovich, M. A.; Lee, J. K. The Acidity of Uracil from the Gas Phase to Solution: The Coalescence of the N1 and N3 Sites and Implications for Biological Glycosylation. *J. Am. Chem. Soc.* **2000**, *122*, 6258–6262.

36. Lin, N.; Dmitriev, A.; Weckesser, J.; Barth, J. V.; Kern, K. Real-Time Single-Molecule Imaging of the Formation and Dynamics of Coordination Compounds. *Angew. Chem., Int. Ed.* **2002**, *41*, 4779–4783.

37. Barth, J. V.; Weckesser, J.; Lin, N.; Dmitriev, A.; Kern, K. Supramolecular Architectures and Nanostructures at Metal Surfaces. *Appl. Phys. A: Mater. Sci. Process.* **2003**, *76*, 645–652.

38. Tait, S. L.; Langner, A.; Lin, N.; Stepanow, S.; Rajadurai, C.; Ruben, M.; Kern, K. One-Dimensional Self-Assembled Molecular Chains on Cu(100): Interplay between Surface- Assisted Coordination Chemistry and Substrate Commensurability. *J. Phys. Chem. C* **2007**, *111*, 10982–10987.

39. Klappenberger, F.; Weber-Bargioni, A.; Auwärter, W.; Marschall, M.; Schiffrin, A.; Barth, J. V. Temperature Dependence of Conformation, Chemical State, and Metal-Directed Assembly of Tetrapyridyl-Porphyrin on Cu(111). *J. Chem. Phys.* **2008**, *129*, 214702.

40. Eichberger, M.; Marschall, M.; Reichert, J.; Weber-Bargioni, A.; Auwärter, W.; Wang, R. L. C.; Kreuzer, H. J.; Pennec, Y.; Schiffrin, A.; Barth, J. V. Dimerization Boosts One-Dimensional Mobility of Conformationally Adapted Porphyrins on a Hexagonal Surface Atomic Lattice. *Nano Lett.* **2008**, *8*, 4608– 4613.

41. Lin, N.; Payer, D.; Dmitriev, A.; Strunskus, T.; Wöll, Ch.; Barth, J. V.; Kern, K. Two-Dimensional Adatom Gas Bestowing Dynamic Heterogeneity to Surfaces. *Angew. Chem., Int. Ed.* **2005**, *44*, 1488–1491.

42. Chen, Q.; Richardson, N. V. Surface Facetting Induced by Adsorbates. *Prog. Surf. Sci.* **2003**, *73*, 59–77.

43. McNutt, A.; Haq, S.; Raval, R. RAIRS High Temperature Phase of the DNA Base Thymine on Cu(110): a Resonance Delocalised Bonding System. *Surf. Sci.* **2002**, *502–503*, 185–192.

44. Schiffrin, A.; Riemann, A.; Auwärter, W.; Pennec, Y.; Weber-Bargioni, A.; Cvetko, D.; Cossaro, A.; Morgante, A.; Barth, J. V. Zwitterionic Self-Assembly of L-Methionine Nanogratings on the Ag(111) Surface. *Proc. Natl. Acad. Sci. U. S. A.* **2007**, *104*, 5279–5284.

45. Schiffrin, A.; Reichert, J.; Pennec, Y.; Auwärter, W.; Weber-Bargioni, A.; Marschall, M.; Dell'Angela, M.; Cvetko, D.; Bavdek, G.; Cossaro, A.; et al. Self-Assembly of L-Methionine on Cu(111): Steering Chiral Organization by Substrate Reactivity and Thermal Activation. *J. Phys. Chem. C* **2009**, *113*, 12101–12108.

46. Horcas, I.; Fernández, R.; Gómez-Rodríguez, J. M.; Colchero, J.; Gómez-Herrero, J.; Baro, A. M. WSXM: A Software for Scanning Probe Microscopy and a Tool for Nanotechnology. *Rev. Sci. Instrum.* **2007**, *78*, 013705.

47. Téoule, R. Radiation-Induced DNA Damage and Its Repair. *Int. J. Radiat. Biol.* **1987**, *51*, 573–589.

48. Perdew, J. P.; Burke, K.; Ernzerhof, M. Generalized Gradient Approximation Made Simple. *Phys. Rev. Lett.* **1996**, *77*, 3865–3868.

49. Lee, K.; Murray, E. D.; Kong, L.; Lundqvist, B. I.; Langreth, D. C. Higher-Accuracy van der Waals Density Functional. *Phys. Rev. B* **2010**, *82*, 081101.

50. Cooper, V. R. Van der Waals Density Functional: An Appropriate Exchange Functional. *Phys. Rev. B* **2010**, *81*, 161104.

51. Giannozzi, P.; Baroni, S.; Bonini, N.; Calandra, M.; Car, R.; Cavazzoni, C.; Ceresoli, D.; Chiarotti, G. L.; Cococcioni, M.; Dabo, I.; et al. QUANTUM ESPRESSO: A Modular and Open-Source Software Project for Quantum Simulations of Materials. *J. Phys.: Condens. Matter* **2009**, *21*, 395502.

52. Vanderbilt, D. Soft Self-Consistent Pseudopotentials in a Generalized Eigenvalue Formalism. *Phys. Rev. B* **1990**, *41*, 7892–7895.

53. Kresse, G.; Furthmüller, J. Efficiency of Ab-Initio Total Energy Calculations for Metals and Semiconductors Using a Plane-Wave Basis Set. *Comput. Mater. Sci.* **1996**, *6*, 15–50.

54. Blöchl, P. E. Projector Augmented-Wave Method. *Phys. Rev. B* **1994**, *50*, 17953–17979.